Hybrid thermochemical cycles for low-grade heat storage and conversion into cold and/or power

Alexis Godefroy, Maxime Perier-Muzet, Pierre Neveu, Nathalie Mazet

Hybrid thermochemical cycles for low-grade heat storage and conversion into cold and/or power

Alexis Godefroy[a,b], Maxime Perier-Muzet[a,b], Pierre Neveu[b] and Nathalie Mazet[a*]

[a] CNRS-PROMES Laboratoire PROcédés, Matériaux et Energie Solaire, 66100 Perpignan, France
[b] UPVD Université de Perpignan Via Domitia, 66100 Perpignan, France
** Corresponding author: mazet@univ-perp.fr*

Abstract:

This paper investigates several new hybrid cycles combining a solid/gas sorption refrigeration cycle with a Rankine cycle, and targeting three key functions: they are able to recover low-grade heat (for instance industrial waste heat), to store this energy, and to convert it into cold and/or power. Five operating modes have been designed, for either prevailing cold production or power generation. A thermodynamic analysis was performed to evaluate their energy and exergy performances, for a wide variety of reactive salts in the thermochemical system. Depending on the different modes and reactants, these hybrid thermochemical cycles can operate at temperatures as low as 87 °C. The share of power in total energy production lies between 0 and 30% for prevailing cold production modes, and between 50 and 100% for prevailing power generation modes. The energy and exergy efficiency reach 0.61 and 0.41, respectively. The energy storage density reaches about 170 kWh per m^3 of storage system. In some cases, additional power generation occurs during the charging step. Alternative systems performing the same functions and based on commercial systems have been designed and compared with hybrid thermochemical cycles. This comparison highlights that the energy storage density is lower for hybrid cycles. However, the global energy efficiency can be higher for hybrids, especially for prevailing cold production modes where it can be 34 % higher than for the alternative commercial system.

Keywords:
Thermochemical cycles, Hybrid sorption cycles, Power and cold cogeneration, Thermal energy storage, Low-grade heat recovery.

1. Introduction

As regards both energy demand and resources, the management of variability is a decisive issue; this topic covers variability in energy form (which can be addressed through developing multi-purpose systems) and time-variability (which can be addressed through integrating energy storage systems).

In this context, an interesting option consists in pooling devices of two thermodynamic cycles, in order to combine their functionalities and build a so-called “hybrid” system. This may lead to a substantial improvement in flexibility and efficiency. To that end, the most relevant cycles are:

1. Three-temperatures cycles involving a liquid/gas sorption process (absorption). Using evaporation/condensation of a vapor flow and its absorption/desorption in a liquid solution (typically H_2O/LiBr), they take advantage of the related thermal effects (either exo- or endothermal effect, according to the component). Since the liquid solution flows between vapor desorber and absorber, a continuous cold (at the evaporator) or heat (at the absorber) production is achieved. These systems are characterized by quite good Coefficients Of Performance (COP): from 0.7 to 1.
2. Three-temperatures cycles involving a solid/gas sorption process (thermochemical). Although the operating mode is similar to liquid/gas absorption cycles, it is based on a reversible solid/gas

chemical reaction (exothermal synthesis/endothermal decomposition). Hence, these cycles are discontinuous: an intrinsic storage feature is provided, with high energy densities [1]. Moreover, they can operate in a wide range of operating conditions (T, P) depending on the reactive pair [2].

3. Two-temperatures power cycles: Organic Rankine Cycles (ORC) provide an efficient mechanical energy production from a low-grade heat source. Adjusting the working fluid and components allows optimizing the mechanical work production [3]. Further details on ORC modelling are provided in Appendix A.

Both of these three cycles involve a working fluid undergoing state changes in vapor generators and absorbers (evaporator/condenser, desorber/absorber, sorption reactors). Consequently, coupling and hybridizing them will consist in coupling these common components.

Considering the three-temperatures liquid/gas absorption cycle and the two-temperatures power cycle, several hybrid configurations were proposed:

- Firstly, Kalina cycle (power cycle developed from the late 1970s) involves a binary mixture as working fluid (typically NH_3/H_2O) in order to decrease thermodynamic irreversibility caused by temperature mismatch during heat transfer. With a hot source temperature of 399 °C, its energy efficiency ranges from 0.15 to 0.20 and exergy efficiency is approximately 0.52 [4].
- Later, Goswami et al. [5-6] proposed an absorption power cycle providing additional cold production. For this system, providing cold at -10 °C using a 140 °C hot source temperature, energy efficiency ranges from 0.17 to 0.24 while exergy efficiency ranges from 0.49 to 0.65. A review of ORC, Kalina and Goswami cycles was proposed by Karimi et al. [7].
- Kordlar et al. [8] achieved an exergoeconomic analysis of a novel cooling and power cogeneration system based on ORC and absorption refrigeration cycle, using ammonia as the working fluid. Driven by geothermal hot water at 133 °C, their cycle provides cold at 5 °C, with a heat sink temperature at 25 °C. Optimization processes were carried out, using three performance criteria (energy efficiency, exergy efficiency and total products cost). Optimal energy and exergy efficiencies range from 0.25 to 0.29 and from 0.28 to 0.36, respectively.
- Finally, a combined power and cooling system based on ammonia-water absorption refrigeration cycle and Kalina power cycle was recently investigated by Higa et al. [9]. Their hybrid cycle is able to reduce exergy destructions compared with absorption refrigeration cycle. For 253 °C hot source and 30 °C heat sink temperatures, cold is provided at a very low temperature (-54 °C), and the cycle energy and exergy efficiencies range from 0.35 to 0.42 and from 0.32 to 0.47, respectively.

Considering the three-temperatures thermochemical cycle and the two-temperatures power cycle, very few hybrid configurations have been studied despite the interesting storage feature of thermochemical cycles. Most of these investigations have been carried out on resorption cycles (defined hereafter, see Section 2.2) and they are based on the use of ammonia, both as reactive vapor of the solid/gas sorption process and as working fluid of the expansion process.

- For power production only, a resorption cycle implementing a novel composite sorbent was investigated by Jiang et al. [10]. Using hot source at 80-110 °C and heat sink at 30 °C, its energy and exergy efficiencies range from 0.07 to 0.12 and from 0.40 to 0.74, respectively. To overcome the technical limitations of ammonia expansion (wet fluid), Bao et al. [11] proposed a resorption power cycle involving several (2 to 4) expansion stages. Under hot source temperature between 30 and 150 °C and heat sink at 25 °C, energy efficiency and specific work output range from 0.06 to 0.15 and from 100 to 600 kJ/kg_{NH3}, respectively.
- For power and cold cogeneration, one of the first resorption cycles was proposed by Wang et al. [12], and later improved by Lu et al. [13]. Providing cold at 10 °C with a hot source temperature of 110 °C, its COP ranges from 0.83 to 0.93 while exergy efficiency ranges from 0.32 to 0.41. The theoretical and experimental works of Jiang et al. [14-15] lead to energy and exergy efficiencies in the ranges [0.29; 0.42] and [0.12; 0.16] respectively (hot source between 120 and 170 °C, cold production at 10 °C). Moreover, an innovative hybrid cycle based on

solid/gas chemical reaction was proposed by Bao et al. [16] for the cogeneration of power and cold. COP and exergy efficiencies are respectively in the ranges [0.34; 0.57] and [0.20; 0.62] (hot source between 85 and 255 °C, cold production at -10 °C).

Finally, we note that very different sets of assumptions are considered in the literature, especially for temperature pinches. This leads to very different energy and exergy performances: for example, the temperature deviations from solid/gas chemical reaction equilibrium are accounted for in [16], while the studies [12-13] assume that chemical reaction takes place at thermodynamic equilibrium conditions. The influence of equilibrium drops on cycle performances was further investigated by Jiang et al. [17]: a resorption refrigeration unit was built and experimental COP and Specific Cooling Power (SCP) were in the ranges [0.18; 0.27] and [34; 57 $W/kg_{reactants}$], respectively. These values were much lower than the theoretical values computed under equilibrium assumptions: [0.32; 0.45] and [161; 183 $W/kg_{reactants}$], respectively. For this experiment, the operating conditions were: 0 °C cold production, 30 °C heat sink temperature and 115-135 °C hot source temperature.

In this paper, innovative hybrid thermochemical cycles for low-grade heat storage and cogeneration of power and cold are investigated using a new methodology, which underlines the sensitivity of the performances to a wide variety of reactive salts. Firstly, the working principle of hybrid thermochemical cycles is presented (components and thermodynamic paths), which allows identifying five operating modes for these cycles. Then, the framework of the thermodynamic study (assumptions, methodology, performance criteria and indicators) is depicted. In the following section, performance results of hybrid cycles are gathered for hot source temperatures under 250 °C. A comparison with combinations of commercial systems achieving the same features (low-grade heat storage and cogeneration of power and cold) is provided. Finally, conclusions are drawn on advantages, weaknesses and possible applications of the five operating modes of hybrid thermochemical cycles in the fields of low-grade heat storage and conversion.

2. Hybrid cycles for cold and/or power production

2.1. Working principle: general overview

Hybridizing a thermochemical refrigeration cycle with a power cycle leads to the general scheme of Fig. 1. Since it consumes a solid reactant, this system is intrinsically discontinuous: its operation is divided into two steps.

- The charging step (step 1) occurs when a heat source is available (high pressure levels).
- The discharging step (step 2) is performed when a useful effect is needed.

This characteristic provides the **storage function** of the cycle.

The hybrid cycle involves two main components, which swap their roles at each working step:

- A vapor generator, involving an endothermal process to generate the vapor: decomposition reaction of a solid reactant (S_r ➔ S_p + G) or evaporation of the liquid working fluid (L ➔ G).
- A vapor absorber, involving an exothermal process: synthesis reaction of a solid reactant (S_p + G ➔ S_r) or condensation of the gaseous working fluid (G ➔ L).

These components exchange heat and vapor flows:

- Regarding **heat flows**, a heat input (Q_{hot}) is required for the high-pressure endothermal process (charging step), while a **cold production** (Q_{cold}) can be ensured by the low-pressure endothermal process operating at a suitable temperature level (discharging step displayed in lower left corner of Fig. 1). Furthermore, heat is rejected at ambient (Q_{amb}) and mid-temperature (Q_m) by respectively, the high- and low-pressure exothermal processes.
- Regarding **mass flows**, in each step, an expander is located between the vapor generator and absorber, to take advantage of the reactive vapor flow leaving the vapor generator and provide the **power production** (W_{dir} and W_{disch}) of the cycle. Several configurations can be considered,

by either actuating the expander or bypassing it, thanks to the valves on Fig. 1. This management of mass flows brings the innovative power production of the hybrid cycle.

Based on the general pattern of Fig. 1, five hybrid cycles (named operating **modes**) are thus defined. They all provide cogeneration of power and cold, with a prevailing production according to the configuration. In the following study, they are split into two sets according to the prevailing target:

(i) Prevailing cold production:

In this case, cold is produced during discharging step by the endothermal vapor generation: therefore, this working step requires low pressure levels (lower left corner (i) of Fig. 1). Power can be generated either in charging, discharging or both steps. Therefore, three modes are available, depending on the actuation of the expander:

- **Separated** power and cold mode: the expander is actuated in charging step only (the discharging step is isobaric, $W_{disch} = 0$). Therefore, power and cold productions are time-shifted: power is generated in charging step while cold is produced in discharging step.
- **Simultaneous** power and cold mode: the expander is actuated in discharging step only (the charging step is isobaric, $W_{dir} = 0$). Therefore, both cold and power are produced in discharging step.
- **Combined** power and cold mode: the expander is actuated in both of the two working steps (both steps are non-isobaric, $W_{dir} \neq 0$ and $W_{disch} \neq 0$). This enables increasing the total power output.

(ii) Prevailing power generation:

In this case, the endothermal component (vapor generator) operates at higher temperature in the discharging step (defined in lower right corner (ii) of Fig. 1): this step is autothermal, since the heat Q_m (released by the vapor absorber) is transferred to the vapor generator. Thus, vapor generator pressure and temperature are increased, so that the endothermal vapor generation does not provide cold anymore, but power production is increased. However, a residual cold production can be obtained due to the low temperature of the working fluid at the outlet of the expander (see Section 2.2). Since power production can be ensured either in discharging step only or in both steps, two operating modes arise:

- **Discharge** power generation mode: the expander is actuated in discharging step only (isobaric charging step, $W_{dir} = 0$).
- **Combined** charge and discharge power generation mode: the expander is actuated in both charging and discharging step (non-isobaric steps, $W_{dir} \neq 0$ and $W_{disch} \neq 0$), so that the total power generation is increased.

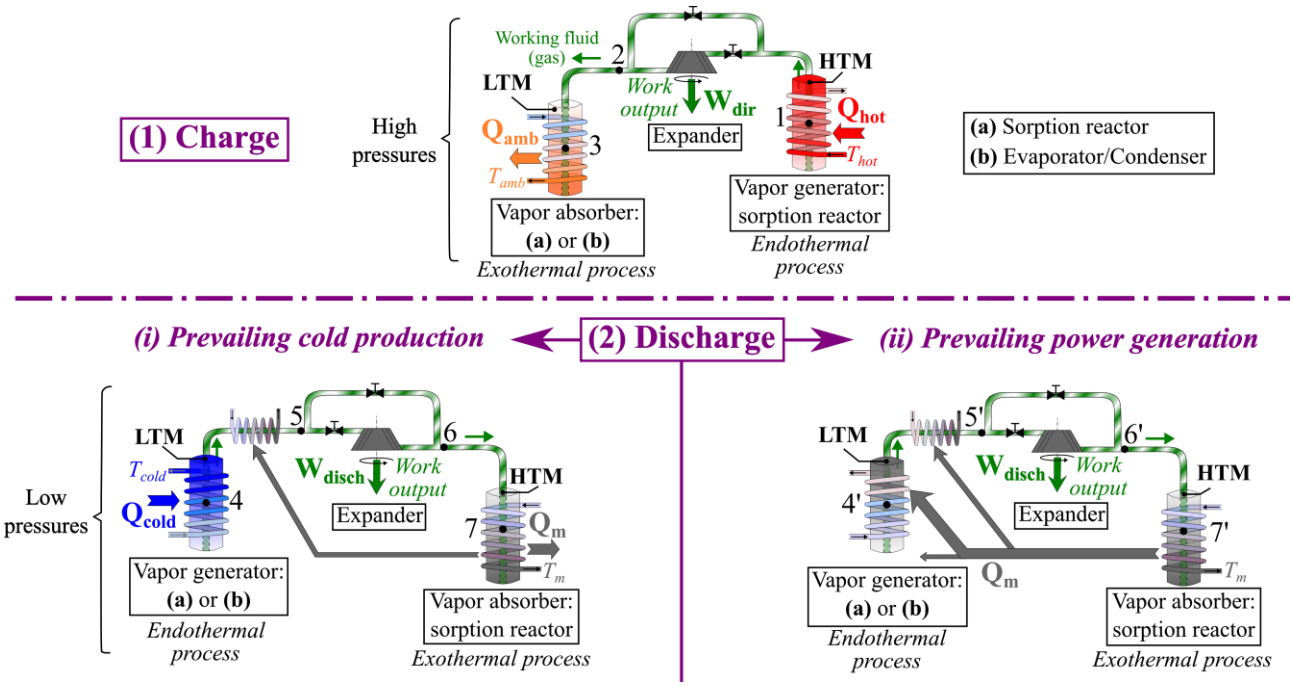

Figure 1. Working principle of hybrid thermochemical cycles: components, mass and energy flows in each working step (Charge/Discharge). ***(a)*** *Resorption cycle, involving 2 sorption reactors;* ***(b)*** *Single sorption cycle, with only 1 sorption reactor and 1 evaporator/condenser (see Section 2.2)*

Finally, the set of configurations can be extended by choosing the vapor absorber and generator in different ways: in the general working principle of Fig. 1, the right-side component must be a sorption reactor, while the left-side component can be either a sorption reactor (case (a): resorption cycles) or an evaporator/condenser of the working fluid (case (b): single sorption cycles).

2.2. Thermodynamic path

In connection with the working principle displayed in Fig. 1, Fig. 2 shows the thermodynamic cycle followed by the working fluid, ammonia. It provides a Clausius-Clapeyron diagram ($ln(P/P^0)$ as a function of $-1/T$), well known for thermochemical systems. In this diagram, the hybrid thermochemical cycle operation is based on two thermodynamic equilibrium lines:

- The High Temperature equilibrium is associated to the High Temperature Material (HTM), which is a solid reactive salt. This is a reversible chemical reaction equilibrium.
- The Low Temperature equilibrium relates to the Low Temperature Material (LTM), which is:
  - Either a solid reactive salt. This case is named a **resorption** cycle: the Low Temperature equilibrium is a chemical reaction equilibrium (referred to as case **(a)** in Fig. 1).
  - Or ammonia. This case is named a **single sorption** cycle: the Low Temperature equilibrium is a liquid/vapor equilibrium (referred to as case **(b)** in Fig. 1).

Fig. 2 highlights the non-isobaric steps in all the modes under consideration.

All the operating modes presented in Section 2.1 can be described using such Clausius-Clapeyron diagrams: both the three modes for prevailing cold production (separated, simultaneous and combined modes) and the two modes for prevailing power production (discharge and combined modes), depending on whether charging and discharging steps are isobaric or not.

Only two typical examples of operating modes are detailed below:

- For prevailing cold production, in combined power and cold mode:
  - In the charging step (upper part of Fig. 2), heat supply (Q_{hot}) drives the endothermal desorption of ammonia, which is released close to the HTM equilibrium conditions (point 1). The reactive fluid is then expanded (between points 1 and 2) and finally condensed or absorbed (point 3).

- In the discharging step (lower left corner (i) of Fig. 2), the endothermal evaporation or desorption of ammonia at a lower pressure (point 4) provides the cooling effect (Q_{cold}); ammonia vapor is superheated (between points 4 and 5), then expanded (between points 5 and 6) and finally absorbed (point 7).

- For prevailing power generation, in combined charge and discharge mode:
  - The charging step is also non-isobaric (upper part of Fig. 2), as described above.
  - In the discharging step, the difference from the three prevailing cold production modes lies in the autothermal operation (lower right corner (ii) of Fig. 2). Indeed, exothermal synthesis heat Q_m (released at point 7') is used to achieve endothermal vapor generation (point 4') and superheating of the generated vapor (between points 4' and 5') upstream of the expander. Therefore, temperature $T_{4'}$ and pressure $P_{high,D}$ increase, allowing a higher power generation instead of cold production. However, we note that a residual cold production can be obtained if the temperature of the working fluid at the expander outlet (point 6') is low enough.

More details on the operation of thermochemical cycles can be found in [18] and [19].

We note that ammonia liquid-vapor equilibrium is modelled by Eq. (1), while chemical reaction equilibrium is modelled by Eq. (2). Those equations are represented by straight lines in the Clausius-Clapeyron diagram (Fig. 2). $\Delta_r H^0$ and $\Delta_r S^0$ are thermodynamic properties of the reactive pairs. $\Delta_r H^0$ imposes the slope of the equilibrium straight line, while $\Delta_r S^0$ fixes its position relative to the ammonia liquid-vapor saturation line. Consequently, the choice of HTM is a decisive factor for the hot source temperature.

$$ln\left(\frac{P}{P^0}\right) = -\frac{L_{vap}}{R.T} + \frac{\Delta S_{vap}}{R} \quad (1)$$

$$ln\left(\frac{P}{P^0}\right) = -\frac{\Delta_r H^0}{R.T} + \frac{\Delta_r S^0}{R} \quad (2)$$

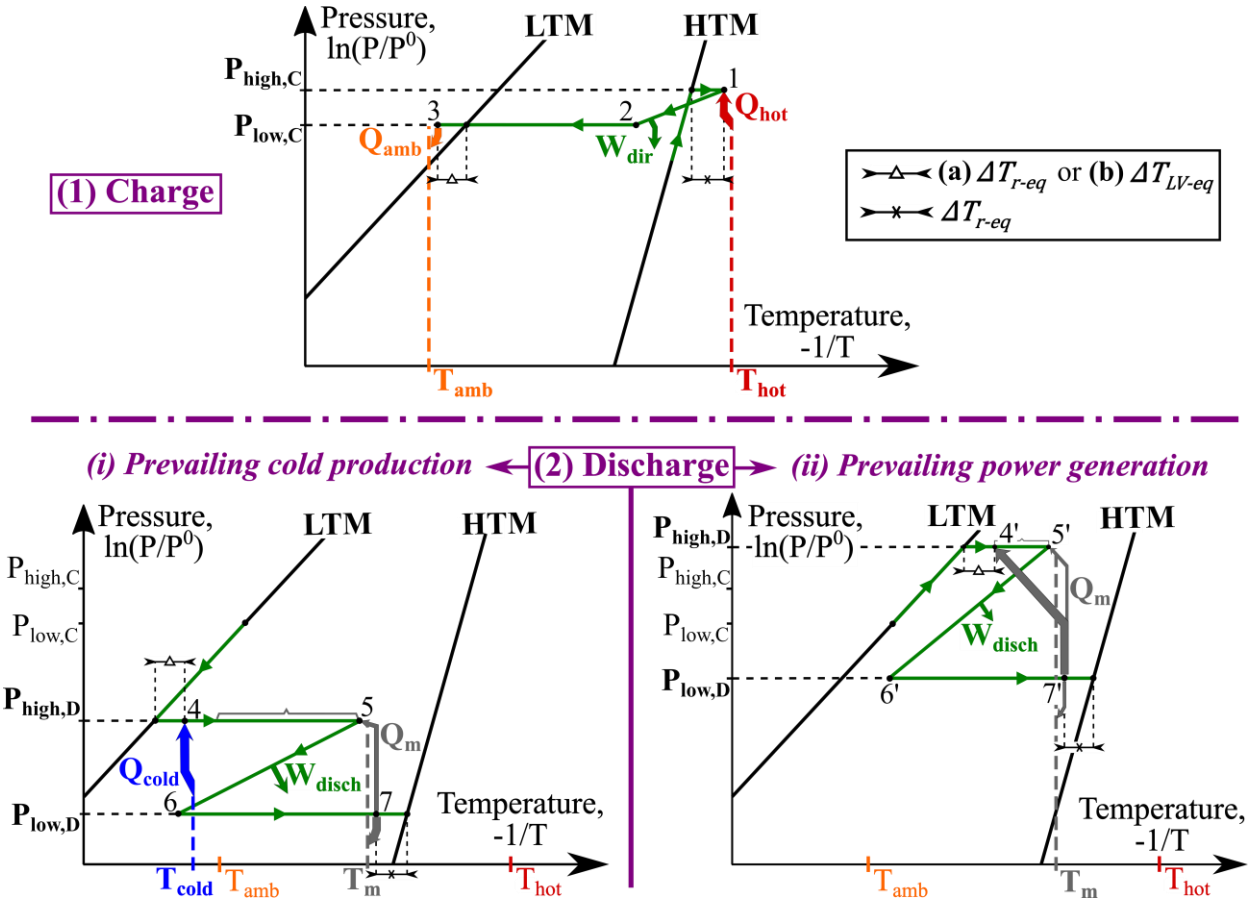

Figure 2. Thermodynamic path followed by the working fluid of a hybrid thermochemical cycle: Clausius-Clapeyron diagram.

3. Thermodynamic study

3.1. Definition of the thermodynamic cycles

This section aims to introduce the main operating conditions and assumptions that have been set to define the thermodynamic states of the working fluid at key points of the cycles.

3.1.1. Operating conditions and main assumptions

The framework of the thermodynamic study is defined by two operating temperatures $T_{cold} = 0$ °C and $T_{amb} = 20$ °C, and a maximal hot source temperature set at $T_{hot,max} = 250$ °C since this work focuses on low-grade heat sources.

The main thermodynamic assumptions are listed below:

- The hybrid cycles operate in steady state
- The isentropic efficiency of expanders is $\eta_{is} = 0.8$.
- Heat transfers with (external or internal) heat sources and sinks are non-equilibrium processes: therefore, several temperature pinches are defined.
  - Temperature pinch for (liquid/liquid) or (liquid/vapor) heat exchange is $\Delta T_{HX1} = 5$ K.
  - Temperature pinch for (vapor/vapor) heat exchange is $\Delta T_{HX2} = 10$ K.
- Temperature deviations from thermodynamic equilibrium lines (LTM or HTM) are also defined. The assigned value of this parameter ΔT_{eq} varies according to the thermodynamic equilibrium:
  - The temperature deviation from thermodynamic equilibrium which is required for a chemical reaction to proceed is $\Delta T_{r\text{-}eq} = 20$ K.

- The temperature deviation required for a liquid/vapor phase change to proceed is $\Delta T_{LV\text{-}eq} = 0$ K, because phase change is not rate-limiting in this system.

- Reference temperature for exergy calculations is $T^0 = T_{amb} = 20$ °C.
- The pressure drops are neglected.
- Heat exchanges between components and the surroundings are neglected
- The maximum reaction advancement range is set at $\Delta X = 0.8$ and the dead volume of the reactor (including porosity of the reactive composite) is set at 50 % of its total volume.

Besides, several technological boundary values are set:

- Working fluid pressure is bounded by $P_{min} = 0.1$ bar and $P_{max} = 30$ bar, for the sake of technical feasibility with acceptable costs.
- A minimal vapor quality $x_{min} = 0.8$ is required at the outlet of the expander.
- The volumetric ratio for expanders is limited to a maximal value $R_{v,max} = 10$, to comply with their nominal operating range (scroll expanders are particularly targeted, as they are suitable for small facilities). For example, R_v is defined as $R_v = v_6/v_5$ (or $R_v = v_{6'}/v_{5'}$) in the discharging steps of Fig. 2. Additional expansion stages (i.e. additional expansion devices) can be added to comply with this constraint.

Finally, this study is restricted to ammonia-salt reactive pairs in the thermochemical reactor. Thus, the working fluid of the whole hybrid thermochemical cycle is ammonia.

3.1.2. Setting process of the thermodynamic cycles

Based on Fig. 2, the main steps for setting the thermodynamic states of ammonia at key points of the cycle are outlined below. This case study refers to the example of combined power and cold mode.

In the charging step:

- The thermodynamic state of ammonia at point 1 and the expansion process 1-2 are governed by Eqs. (3) and (4).
- The cooling process 2-3 is isobaric, and temperature T_2 is set as low as possible while ensuring that the high pressure $P_{high,C}$ remains lower than P_{max}.
- The low pressure $P_{low,C}$ is deduced from heat sink temperature (T_{amb}) and temperature pinches ΔT_{HX1} and ΔT_{eq}, according to Eqs. (5) and (6).
- Finally, the required hot source temperature T_{hot} is deduced from T_1 and temperature pinch ΔT_{HX1}, according to Eq. (7).

$$P_1 = P_{high,C} = P_{eq,HTM}\left(T_1 - \Delta T_{eq}\right) \quad (3)$$

$$h_2 = h_1 + \eta_{is}.\left(h_{2,is} - h_1\right) \quad (4)$$

$$T_3 = T_{amb} + \Delta T_{HX1} \quad (5)$$

$$P_3 = P_{low,C} = P_{eq,LTM}\left(T_3 + \Delta T_{eq}\right) \quad (6)$$

$$T_{hot} = T_1 + \Delta T_{HX1} \quad (7)$$

In the discharging step:

- The high pressure $P_{high,D}$ is deduced from cold source temperature (T_{cold}) and temperature pinches ΔT_{HX1} and ΔT_{eq}, according to Eqs. (8) and (9).
- The low pressure $P_{low,D}$ is set so that the exothermal vapor absorption (point 7) takes place at a temperature higher than T_{amb}, in order to enable heat release: see Eq. (10).
- Temperatures T_7, T_5 and T_m are deduced from $P_{low,D}$ and temperature pinches ΔT_{HX1}, ΔT_{HX2} and ΔT_{eq}, as shown by Eqs. (11), (12) and (13).
- Finally, the expansion process 5-6 is governed by Eq. (14).

$$T_4 = T_{cold} - \Delta T_{HX1} \quad (8)$$

$$P_4 = P_{high,\mathrm{D}} = P_{eq,LTM}\left(T_4 - \Delta T_{eq}\right) \quad (9)$$

$$P_7 = P_{low,D} = max\left(P_{min}; P_{eq,HTM}\left(T_{amb} + \Delta T_{eq}\right)\right) \quad (10)$$

$$T_7 = T_{eq,HTM}(P_7) - \Delta T_{eq} \quad (11)$$

$$T_5 = T_7 - \Delta T_{HX2} \quad (12)$$

$$T_m = T_7 - \Delta T_{HX1} \quad (13)$$

$$h_6 = h_5 + \eta_{is}.\left(h_{6,is} - h_5\right) \quad (14)$$

Note that this study assumes that vapor generation and absorption are non-equilibrium processes, through the determination of operating pressures (Eqs. (3), (6), (9), (10)).

3.2. Methodology

All calculation processes described hereafter have been carried out with EES software [20].

3.2.1. Screening over a panel of reactive salts

This thermodynamic study is based on energy calculations. All extensive quantities related to each cycle (Q_{hot}, Q_{cold}, masses, volumes, …) are computed for a given electrical production ($W = W_{dir} + W_{disch} = 1$ kWh). On the other hand, all specific values are reported to the mass of working fluid required for a whole cycle.

This work aims at exploring the potential of hybrid thermochemical cycles presented in Section 2 for different solid reactive salts, and to retrieve the most promising ones. A database containing thermochemical data (reaction enthalpy $\Delta_r H^0$ and reaction entropy $\Delta_r S^0$) for 103 reactive ammonia salts is used. These data come from values collected and computed by Touzain [21] and from CNRS-PROMES knowledge. Non-environmental friendly salts (Pb) and salts having low stoichiometries have been excluded. The remaining salts are mainly metallic chlorides, bromides and iodides, for instance: $CaCl_2$, $MnCl_2$, $FeBr_2$, SrI_2.

The methodology of this study is divided into two main steps:

- Firstly, the LT equilibrium is set: it is either a chemical reaction equilibrium (for resorption cycles), or an ammonia liquid/vapor equilibrium (for single sorption cycles).
- Secondly, for each one of the 103 reactive salts, its data ($\Delta_r H^0$, $\Delta_r S^0$) are used to define the HT equilibrium, and the thermodynamic path (i.e. pressure, temperature, specific enthalpy and entropy at each key point of the cycle) is computed

Note that, in the case of resorption cycles, a solid reactive salt has to be chosen as LTM in the first step. For all resorption cycles presented in the next sections, $BaCl_2$ (8/0)NH_3 is chosen as LTM since it enables cold production at $T_{cold} = 0$ °C with a decomposition reaction pressure (see Fig. 2) $P_{high,D} = P_4 = 0.09$ bar , which is considered as acceptable despite the boundary value $P_{min} = 0.1$ bar.

3.2.2. Relevant performance criteria

For each LTM-HTM pair, given their thermodynamic equilibria, and for $W = 1$ kWh, the following quantities are computed:

- Hot source temperature T_{hot} (depending on the HTM and temperature pinches).
- Volumetric expansion ratio R_v (or $R_{v,1}$, $R_{v,2}$, … if there are several expansion stages).
- Heat consumption Q_{hot}.
- Cold production Q_{cold}.

Focusing on prevailing cold production modes, a previous work provides further details about these calculations, especially energy balance equations [22]. Regarding prevailing power generation modes, a similar set of equations has been solved.

It is recalled that a residual cold production Q_{cold} can occur in the autothermal discharging step of prevailing power generation modes, thanks to the low temperature reached by the working fluid at the expander outlet: even if this is not the prioritized useful effect for these operating modes, it is taken into account in the cycle performances.

In order to pick out the most relevant reactive salts, three performance criteria are defined and computed for each HTM:

- Energy efficiency,

$$\eta_I = \frac{W + Q_{cold}}{Q_{hot}} \tag{15}$$

- Exergy efficiency,

$$\eta_{ex} = \frac{W + Ex_{cold}}{Ex_{hot}} \tag{16}$$

, with $$Ex_{hot} = Q_{hot}.\left(1 - \frac{T^0}{T_{hot}}\right) \tag{17}$$

and $$Ex_{cold} = Q_{cold}.\left(\frac{T^0}{T_{cold}} - 1\right) \tag{18}$$

- Power production ratio,

$$\tau_w = \frac{W}{W + Q_{cold}} \tag{19}$$

These performance criteria are relevant because they give enough information to provide a fair comparison between the cogeneration cycles presented in this study. Indeed:

- The energy efficiency η_I, defined in Eq. (15), is the ratio of useful energy to input energy. This is a cogeneration efficiency, which allows comparison with other cogeneration cycles working under the same temperatures (T_{cold}, T_{amb}, T_{hot}).
- The exergy efficiency η_{ex} (Eq. (16)) is the ratio of useful exergy to input exergy. It accounts for the fact that mechanical work and heat do not have the same "quality", by weighting the energy using the Carnot factors related to T_{hot} (according to Eq. (17)) and T_{cold} (according to Eq. (18)).
- The power production ratio τ_w (Eq. (19)) enables computing the specific work output w (see Eq. (20)). It should be read alongside η_I, whose order of magnitude greatly depends on the useful effects (cold and/or power).

$$w = \frac{\eta_I.\tau_w.(w + ex_{cold})}{\eta_{ex}.\left(1 - \frac{T^0}{T_{hot}}\right)} \tag{20}$$

Once the computations are completed for all reactive salts, a first selection is carried out: reactive salts and thermodynamic cycles that cannot meet the technological boundary values $R_{v,max}$, x_{min}, P_{min}, P_{max} or $T_{hot,max}$ are excluded. The remaining salts are ranked according to each of the previous three criteria and, for each of these criteria, only the ten best salts are selected. At the end of this process, about 15 to 30 solid salts are selected for each cycle configuration (see Section 4).

As mentioned in Section 3.1, several expansion stages have to be implemented in some cases in order to fulfill the constraint (maximum value) $R_{v,max}$. Only slight differences were observed between the performances of one- to three-expansion cycles. Consequently, only the configurations with the lowest number of expansion stages (leading to the easiest implementations) are selected in Section 4.

Finally, the storage functionality is analyzed with the Energy Storage Density ESD (Eq. (21)), defined as the ratio between the useful effects produced during discharging step (W_{disch} and Q_{cold}) and the

volume of the storage components of the process (NH_3 tanks and reactors). It allows comparing the storage density of different processes or operating modes.

$$ESD = \frac{W_{disch} + Q_{cold}}{V_{stor}} \quad (21)$$

4. Results and discussions

4.1. Performances

Fig. 3 gathers the results for hybrid thermochemical cycles (5 operating modes): for each mode, the performance criteria of Section 3.2.2 are displayed as a function of the hot source temperature T_{hot} required for each reactive pair. Vertical black lines are added to delimit three areas corresponding to the hot source temperature ranges: [100; 150 °C], [150; 200 °C] and [200; 250 °C].

Concerning the hot source temperatures required to drive the cycles:

- The discharge power generation mode (red triangles) operates at $T_{hot} > 87$ °C.
- The simultaneous power and cold cogeneration mode (green squares) operates at $T_{hot} > 107$ °C.
- The combined power generation mode (brown rhombuses) operates at $T_{hot} > 117$ °C.
- The separated (blue triangles) and combined (pink circles) power and cold cogeneration modes operate at $T_{hot} > 138$ °C.

These differences can be explained using Fig. 2:

- Pressure $P_1 = P_{high,C}$ is higher in the modes involving a power production in charging step ($W_{dir} \neq 0$): combined power generation mode, separated and combined power and cold cogeneration modes. Indeed, these modes involve a non-isobaric operation in charging step so that (accounting for Eqs. (3) and (7)) the temperatures T_1 and T_{hot} are higher.
- As discharge power generation mode and simultaneous power and cold cogeneration mode do not involve a power production in the charging step, their minimal hot source temperature is lower. However, because of the constraint $P_6 > P_{min}$, all HTMs are not usable to achieve both cold and power production.

We note that for a given operating mode, resorption cycles (filled symbols) require higher hot source temperatures than single sorption cycles (empty symbols) to operate. For example, for the discharge power generation mode, the combined power generation mode and the separated power and cold cogeneration mode, the minimal hot source temperatures in resorption case versus single sorption case are respectively: $T_{hot} = 141$ °C versus 87 °C, $T_{hot} = 183$ °C versus 117 °C, $T_{hot} = 212$ °C versus 138 °C. These differences result from the closeness of LTM and HTM equilibrium lines. Therefore, resorption cycles are unfeasible for a lot of HTMs, especially for the low temperature ones.

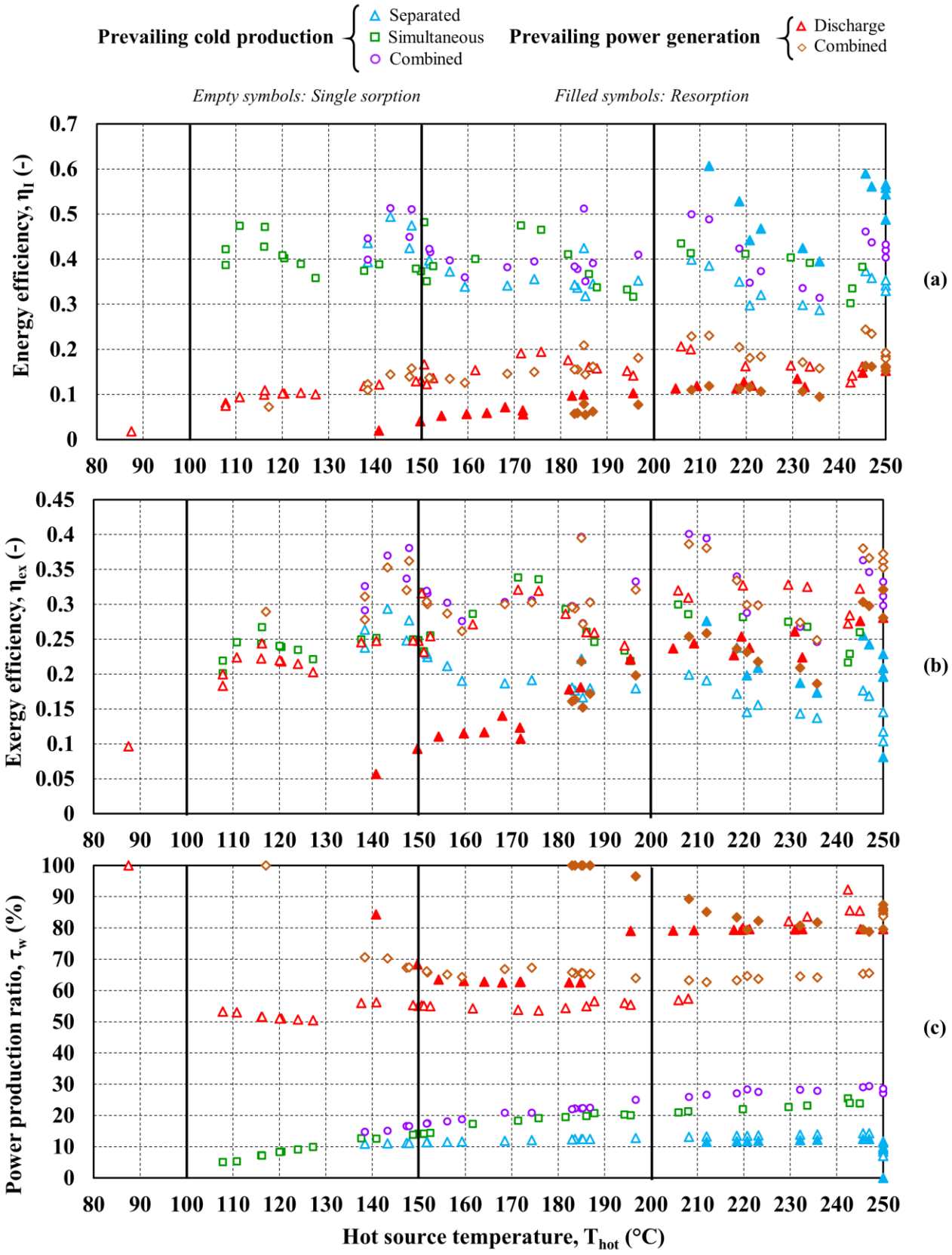

Figure 3. Performance results of the 5 operating modes of the hybrid thermochemical cycles. Energy efficiency (a), exergy efficiency (b) and power production ratio (c).

The power production ratio τ_w is plotted in Fig. 3c, as a support to the following analyses on energy and exergy efficiencies.

Regarding the 1st law energy efficiencies:

- All cogeneration modes show good performances: η_I ranges from 0.28 to 0.61. For power generation modes, the energy efficiency is lower: it reaches 0.21 in discharge mode and 0.24 in combined mode. These differences are related to the share of power and cold in the total energy production: τ_w ranges from 0 to 30 % for cogeneration modes, against 50 to 100 % for power generation modes. A higher share of cold production is always beneficial to the energy efficiency.
- The best values are reached with the resorption cycle in separated cogeneration mode (filled blue triangles). In resorption cases, cold production is higher than in single sorption because it results from the decomposition enthalpy of an ammonia salt, which is higher than the vaporization enthalpy of ammonia ($\Delta_r H^0 \approx 2.L_{vap}$).

Regarding the exergy efficiencies:

- The combined power and cold cogeneration mode shows the best values in each of the three temperature areas: η_{ex} ranges from 0.20 to 0.40. This is due to the fact that power production is higher than in separated or simultaneous cogeneration modes.
- Concerning power generation modes, η_{ex} logically increases with T_{hot}: the pressure ratio $P_{high,D}/P_{low,D}$ increases, favoring the power production. η_{ex} would probably exceed exergy performances of the combined cogeneration mode if hot source temperatures higher than $T_{hot,max}$ were considered.

Finally, the most performant systems are retrieved for each temperature area from Fig. 3:

- As regards energy efficiency, combined power and cold cogeneration mode exhibits the best performance in areas [100; 150 °C] ($\eta_I = 0.51$) and [150; 200 °C] ($\eta_I = 0.51$), but the separated power and cold mode in resorption case overtakes it in the area [200; 250 °C] ($\eta_I = 0.61$).
- The highest exergy efficiency is reached by the combined power and cold cogeneration mode in each of the three areas [100; 150 °C] ($\eta_{ex} = 0.38$), [150; 200 °C] ($\eta_{ex} = 0.40$) and [200; 250 °C] ($\eta_{ex} = 0.40$). We note that the best exergy performances of combined power generation mode are very close to those values.

However, it has to be kept in mind that the highest η_I values obtained by hybrid thermochemical cycles results from a high share of cold production in the energy output: these cycles do not provide a full power output (as shown by τ_w values in Fig. 3c). The exergy efficiency η_{ex} has a significant interest to account for the exergy content of the outputs and to extend the analysis and comparison of all these thermodynamic cycles.

Figure 4 is dedicated to analysing the storage function of hybrid cycles thanks to the Energy Storage Density (*ESD*, defined in Eq. (21)). *ESD* is plotted according to the reactive salts because this storage indicator mainly depends on reactant characteristics, such as the reaction stoichiometry and the molar volume of the salt. These salts are ranked on the x-axis according to their thermodynamic equilibrium temperature. The hot source temperatures required in charging steps for each reactive salt are plotted in Figure 5.

As a result of the x-axis choice, the *ESD* values are scattered over a large range.

Firstly, the prevailing cold production modes present significantly higher energy density values than the prevailing power modes, up to 3 times higher. Among them, the simultaneous mode is the best one because all the energy is produced during the discharging step, while in the combined mode, a part of electricity is produced during the charging step and is not accounted for in the *ESD* calculation. Similarly, in the separated mode, all the electricity production occurs in the charging step, leading to lower *ESD* values.

On the other hand, the prevailing power generation modes result in lower *ESD* values than for the prevailing cold production modes. This outcome results from the fact that cold production is higher than power generation, which has already been discussed above in the analysis of energy and exergy efficiencies. In most cases, *ESD* is higher for single sorption cycles than for resorption cycles, because the latter involve a second reactor whose volume is larger than the condensate tank involved in single

sorption cycles. Nevertheless, in some cases (separated power and cold cogeneration mode, blue triangles in Fig. 4), this ranking is reversed because the molar enthalpy of endothermal reaction producing cold is much higher than the molar vaporization enthalpy of ammonia, and this higher enthalpy compensates the large volume of the reactor.

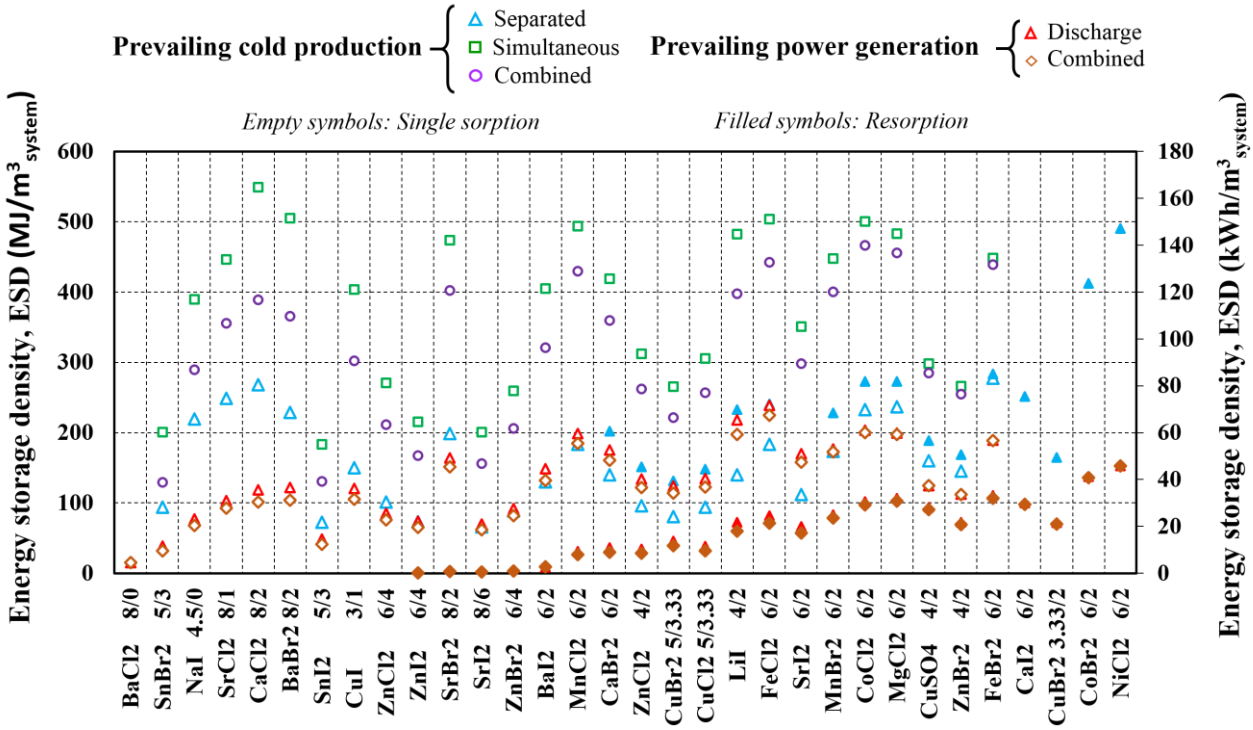

Figure 4. Energy storage density vs reactive salts (HTM). The reference volume is the storage system, including the whole volume of reactors (1 for single sorption, 2 for resorption cases) and the liquid ammonia tank (single sorption case).

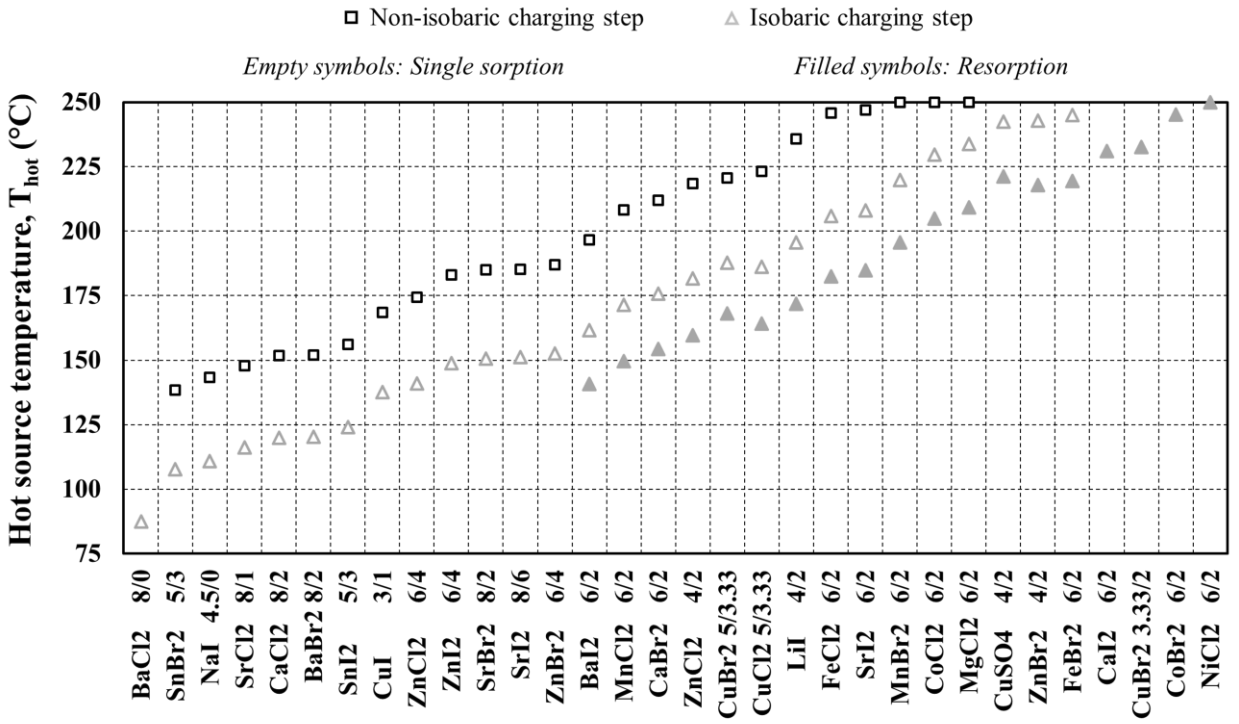

Figure 5. Hot source temperature T_{hot} required for the charging steps. Only 3 cases are plotted because, for a given salt, this temperature only depends on whether the charging step is isobaric or non-isobaric. An isobaric charging step occurs in simultaneous and discharge modes; all other

modes involve non-isobaric charging steps. For the non-isobaric charging step cases, resorption and single sorption temperatures are superposed

4.2. Comparison with alternative systems

4.2.1. Methodology

In order to evaluate the potential of the hybrid thermochemical cycles, a thermodynamic analysis comparison is introduced, considering an alternative system composed by well-known mono-functional thermodynamic cycles that are able to generate the same useful effects as hybrid cycles.

As for thermochemical hybrid cycles, the alternative system is thermally driven, and it has to produce cold and/or electricity and to include a storage function (for electricity and/or cold). The proposed alternative system combines the most common commercial devices (Fig. 6):

- An ORC that is able to convert heat into electricity.
- Electrochemical batteries that insure electricity storage.
- An electrically driven refrigeration machine for cold production.

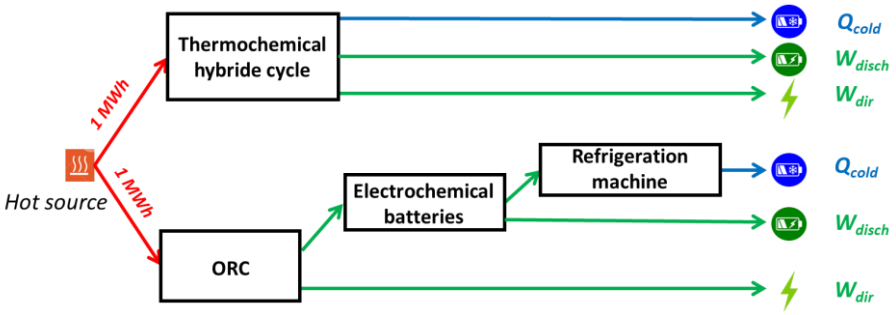

Figure 6: Schematic representation of the energy storage and conversion process of the thermochemical hybrid cycle and the proposed alternative system.

A model has been developed for the alternative system with the same main assumptions as for hybrid cycles analysis, and adding some specific constraints of this system:

- Steady-state operation is assumed.
- The pressure drops and heat exchanges between components and the surroundings are neglected.
- At the evaporator (refrigeration machine) or generator (ORC) outlet, the working fluid is superheated and at the condenser outlet (for both refrigeration machine and ORC), the working fluid is subcooled.
- Isentropic efficiencies are set for compressions and expansions.
- Temperature pinches are defined for heat exchanges with sources.

More details on the modelling of the alternative system (modelling of ORC, electrochemical batteries and refrigeration machine) are provided in Appendix A.

The main simulation parameters are summarized in Table 1.

For each operating mode of hybrid thermochemical cycles, a comparison was performed by first calculating the power production ratio (according to (19)) and the power storage ratio (ratio $W_{disch}/(W_{dir}+W_{disch})$) for the hybrid cycle, then applying these ratios to the alternative system. Moreover, ambient and cold production temperatures were set at the same values: $T_{amb} = 20$ °C and $T_{cold} = 0$ °C.

The comparison is carried out for two case studies: $T_{hot} \approx 150$ °C and $T_{hot} \approx 250$ °C, in order to be representative of a large range of industrial waste heat. The previous analysis (Section 4.1) allows selecting the most promising reactive salts (based on a trade-off between energy efficiency, exergy

efficiency and energy storage density) for each of these two temperatures and each operating mode of hybrid thermochemical cycles, considering only single sorption cycles for technical reasons.

ORC			
	Working fluid	Isopentane	
	Expander isentropic efficiency	0.8	-
	Pump isentropic efficiency	0.9	-
	Temperature pinch at the condenser	5	K
	Subcooling at the condenser	5	K
	Temperature pinch at the generator	10	K
Batteries			
	Charge/Discharge efficiency	0.9	-
	Energy storage density	250	kWh/m^3
	Depth of discharge [23]	0.5	-
Refrigeration Machine			
	Working fluid	R290	
	Compressor isentropic efficiency	0.7	-
	Temperature pinch at the condenser	5	K
	Subcooling at the condenser	5	K
	Temperature pinch at the evaporator	5	K
	Superheating at the evaporator	5	K

Table 1: Main simulation parameters of the alternative system

4.2.2. Results and discussions

Figure 7 illustrates the performance comparison between thermochemical hybrid cycles and the proposed alternative system for two hot source temperatures ($T_{hot} \approx 150$ °C and $T_{hot} \approx 250$ °C).

For this comparative analysis, the selection process led to different reactive salts for the two hot source temperatures. As discussed in Section 4.1, the hybrid cycles performances and power production ratios depend much more on the reactive salt than the hot source temperature. Therefore, the energy efficiencies (Fig. 7a) of the hybrid cycles and even of the alternative system do not always increase with increasing hot source temperature, as expected for power cycles.

For prevailing cold production modes, the hybrid thermochemical cycles efficiencies (energy and exergy) are higher than the alternative system ones, except for separated mode at $T_{hot} = 250$ °C. However, in prevailing power generation modes, the hybrid cycles efficiencies are slightly lower than for the alternative system ones, except for the combined mode at $T_{hot} = 250$ °C.

As expected, the cold energy predominates in prevailing cold production modes, but it is also significant in prevailing power generation modes. Due to the low exergy content of the cold production, in terms of exergy, the power production is predominant whatever the operating mode.

For a given hot source temperature, introducing a non-isobaric charging step (simultaneous to combined power and cold mode, or discharge to combined power mode) requires a change of the reactive salt and leads to an increase in the total power production, but also a decrease in power generation during the discharging step.

Whatever the mode, the energy storage densities of the thermochemical hybrid cycles are lower than for the alternative systems, except for the discharge power generation mode at $T_{hot} = 250$ °C where they are similar. This lower energy storage density has to be balanced with the higher energy

efficiency, and with environmental considerations (better expected recyclability and availability of raw materials) and higher expected lifetime of the thermochemical storage system compared to electrochemical batteries.

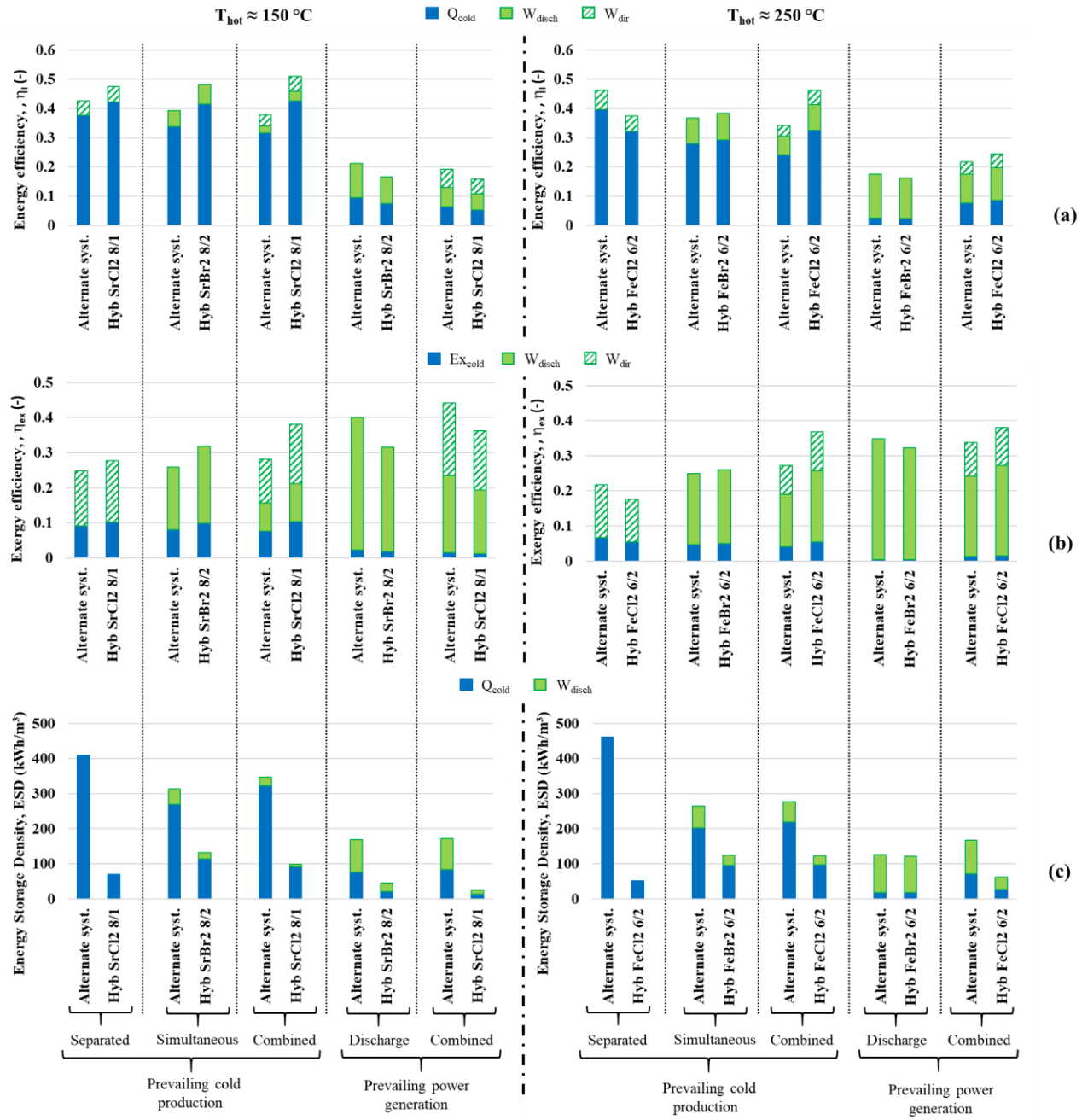

Figure 7: Performance comparison between hybrid thermochemical cycles and alternative system (ORC + electrochemical batteries + refrigeration machine) with the same power production ratio and power storage ratio, for two hot source temperatures: 150 °C (left) and 250 °C (right). T_{amb} = 20 °C and T_{cold} = 0 °C. Energy efficiency (a), exergy efficiency (b) and energy storage density (c).

5. Conclusion

This paper gathers the thermodynamic investigations of new concepts of hybrid thermochemical cycles. These cycles present 3 key features: (i) they can be driven by low-grade heat such as industrial waste heat, at temperatures ranging from 100 to 250°C, (ii) they are able to store this energy as chemical potential, and (iii) they are able to convert it into cold and/or power, providing a cogeneration of power and cold with either prevailing cold production or power generation. Five operating modes have been designed:

- For prevailing cold production: separated power and cold mode (power production during charging step, cold production during discharging step), simultaneous power and cold mode (both productions during discharging step) and combined power and cold mode (power production during both steps, cold production only during discharging step).
- For prevailing power generation: discharge power mode and combined charge and discharge power mode (involving a power production in discharging and both steps, respectively).

A thermodynamic analysis has been carried out to evaluate the performances of these fives hybrid cycles, for a large variety of reactive salts implemented in the thermochemical system. It demonstrates the capability to operate under low-grade heat sources, as low as 87 °C. The part of power in the total energy production ranges from 0 to 30% for prevailing cold production modes, and from 50 to 100% for prevailing power generation modes. The efficiencies reach interesting values: 0.61 for the energy efficiency (in separated power and cold mode) and 0.41 for the exergy efficiency (in combined power and cold mode). This study highlights the most relevant modes according to the targeted application:

- If cold storage and production functions are primarily needed, with low power requirements, separated power and cold cogeneration mode is the most interesting option.
- If power and cold storage and cogeneration functions are desired, combined power and cold mode is the most performant system; however, although slightly less performant, simultaneous mode requires only one expansion device and can operate at lower hot source temperatures.

Regarding the energy storage capability of hybrid cycles, the most interesting modes are logically the cold prevailing modes, reaching about 170 kWh/m^3 of storage system. We note that this storage criterion only takes into account the energy production during the discharging step. Some operating modes (separated, combined) provide an additional power generation during the charging step.

Last, these multifunctional hybrid cycles have been compared to alternative systems fulfilling the same functionalities, by combining several commercial systems: an ORC that can be driven by a low-temperature hot source to provide the power generation, electrochemical batteries to store this electric production, and an electrically driven refrigeration machine for cold production. The results show that the energy storage density is lower for the hybrid cycles than for the alternative system, while efficiencies can be higher with the hybrids especially in prevailing cold production modes. The most promising configurations are the simultaneous and combined modes with prevailing cold production: their energy efficiencies can be 34 % higher than the alternative ones.

The lower energy storage density has to be balanced by other criteria, such as environmental impacts (recyclability, availability of raw materials and lifetime) expected to be better for hybrid thermochemical cycles than electrochemical batteries.

This paper shows the promising thermodynamic performances of hybrid thermochemical cogeneration cycles. An experimental proof of concept is currently developed to demonstrate the feasibility and the controllability of this innovative cycle.

Acknowledgments

Alexis Godefroy receives a PhD grant from the Ministry of Education (doctoral contract n° 2017-09-ED.305, UPVD, Perpignan, France).

Nomenclature

ESD	energy storage density, kWh/m^3
ex	mass density of exergy, J/kg
Ex	exergy, J
H	enthalpy, J
HTM	High Temperature Material
L	molar latent heat, J/mol
LTM	Low Temperature Material
P	pressure, bar

Q	amount of heat, J
R	constant of the ideal gas law, J/(mol.K)
R_v	volumetric expansion ratio, -
S	entropy, J/K
$\mathcal{S}$	molar entropy, J/(mol.K)
S_r	Rich salt (after synthesis reaction)
S_p	Poor salt (after decomposition reaction)
T	temperature, °C
v	specific volume, m^3/kg
V	volume, m^3
w	mass density of mechanical work, J/kg
W	mechanical work, J
x	vapour quality, -
X	Chemical reaction advancement

Greek symbols

Δ	gap
Δ_r	Lewis operator (chemical reaction)
η	efficiency
τ	ratio

Subscripts and superscripts

0	reference state
I	energy-related (1^{st} law)
amb	ambient temperature level
Bat	electrochemical batteries
c	compressor
cold	cold temperature level
cond	condensation
C	charging step
dir	direct production
disch	production in discharging step
D	discharging step
e	expander
eq	thermodynamic equilibrium
evap	evaporation
ex	exergy-related (2^{nd} law)
high	high pressure level
hot	hot temperature level
HX1	liquid/vapor or liquid/liquid heat exchange
HX2	vapor/vapor heat exchange
is	isentropic
low	low pressure level
LV	liquid-vapor phase change
m	medium temperature level

max	maximal value
min	minimal value
ORC	Organic Rankine Cycle
p	pump
r	chemical reaction
Ref	refrigeration machine
stor	storage components
sub	subcooling
sup	superheating
vap	vaporization
w	mechanical work

References

[1] Aydin D., Casey S., Riffat S., The latest advancements on thermochemical heat storage systems, Renewable and Sustainable Energy Reviews 2015;41:367-356.

[2] Cabeza L. F., Solé A., Barreneche C., Review on sorption materials and technologies for heat pumps and thermal energy storage, Renewable Energy 2017;110:39-3.

[3] Ayachi F., Ksayer E. B., Zoughaib A., Neveu P., ORC optimization for medium grade heat recovery, Energy 2014;68:47-56.

[4] Kalina A., Combined cycle and waste heat recovery power systems based on a novel thermodynamic energy cycle utilizing low-temperature heat for power generation. ASME Joint Power Generation Conference; 1983 Sep 25-29; Indianapolis, USA.

[5] Xu F., Goswami D., Bhagwat S., A combined power / cooling cycle, Energy 2000;25:246-233.

[6] Hasan A., Goswami D., Vijayaraghavan S., First and second law analysis of a new power and refrigeration thermodynamic cycle using a solar heat source, Solar Energy 2002;73(5):393-385.

[7] Karimi M., Dutta A., Kaushik A., Bansal H., Haqu S., A review of Organic Rankine, Kalina and Goswami cycle, Int. Journal of Eng. Technology, Management and App. Sciences 2015;3.

[8] Kordlar M. A., Mahmoudi S. M. S., Exergoeconomic analysis and optimization of a novel cogeneration system producing power and refrigeration, Energy Conversion and Management 2017;134:208-20.

[9] Higa M., Yamamoto E. Y., de Oliveira J. C. D., Conceição W. A. S., Evaluation of the integration of an ammonia-water power cycle in an absorption refrigeration system of an industrial plant, Energy Conversion and Management 2018;178:265-76.

[10] Jiang L., Lu Y., Roskilly A., Wang R., Wang L., Tang K., Exploration of ammonia resorption cycle for power generation by using novel composite sorbent, App. Energy 2018;215:467-457.

[11] Bao H., Ma Z., Roskilly A. P., A chemisorption power generation cycle with multi-stage expansion driven by low-grade heat, Energy Conversion and Management 2017;150:956-65.

[12] Wang L., Ziegler F., Roskilly A., Wang R., Wang Y., A resorption cycle for the cogeneration of electricity and refrigeration, Applied Energy 2013;106:64-56.

[13] Lu Y., Wang Y., Bao H., Yuan Y., Wang L., Roskilly A., Analysis of an optimal resorption cogeneration using mass and heat recovery processes, Applied Energy 2015;160:901-892.

[14] Jiang L., Wang L., Zhang X., Liu C., Wang R., Performance prediction on a resorption cogeneration cycle for power and refrigeration with energy storage, Renewable Energy 2015;83;1259-1250.

[15] Jiang L., Wang L., Liu C., Wang R., Experimental study on a resorption system for power and refrigeration cogeneration, Energy 2016;97;190-182.

[16] Bao H., Wang Y., Roskilly A., Modelling of a chemisorption refrigeration and power cogeneration system, Applied Energy 2014;119:362-351.

[17] Jiang L., Wang L. W., Zhou Z. S., Zhu F. Q., Wang R. Z., Investigation on non-equilibrium performance of composite adsorbent for resorption refrigeration, Energy Conversion and Management 2016;119;67-74.

[18] Stitou D., Mazet N., Mauran S., Experimental investigation of a solid/gas thermochemical storage process for solar air-conditioning, Energy 2012;41:270-261.

[19] Fitó J., Coronas A., Mauran S., Mazet N., Stitou D., Definition and performance simulations of a novel solar-driven hybrid absorption-thermochemical refrigeration system, Energy Conversion and Management 2018;175:312-298.

[20] F-Chart Software: Engineering Software EES: Engineering Equation Solver http://www.fchart.com/ees/.

[21] Touzain P., Thermodynamic values of ammonia salts reactions for chemical sorption heat pump. Proceedings of the International Sorption Heat Pump Conference; 1999 Mar 24-26; Munich, Germany.

[22] Godefroy A., Perier-Muzet M., Mazet N., Thermodynamic analyses on hybrid sorption cycles for low-grade heat storage and cogeneration of power and refrigeration, Applied Energy 2019;255.

[23] Guena T., Leblanc P., How Depth of Discharge affects the cycle life of Lithium-Metal-Polymer batteries. Proceedings of the Twenty-Eighth International Telecommunications Energy Conference, INTELEC 06, Providence, RI; 2006:1-8.

Appendix A: Modelling of the alternative system

The alternative system is composed by an organic Rankine cycle, electrochemical batteries and an electrically driven vapour compression chiller. The thermodynamic performances of this system have been determined with a simulation tool specifically developed with the EES software, implementing the following main equations.

Organic Rankine Cycle

In the ORC the working fluid is expanded in a turbine, where mechanical work is produced, then it is condensed and subcooled in the condenser. The liquid working fluid is then pressurized by means of a pump and it finally undergoes vaporization and superheating in a boiler (thanks to the low-grade heat source).

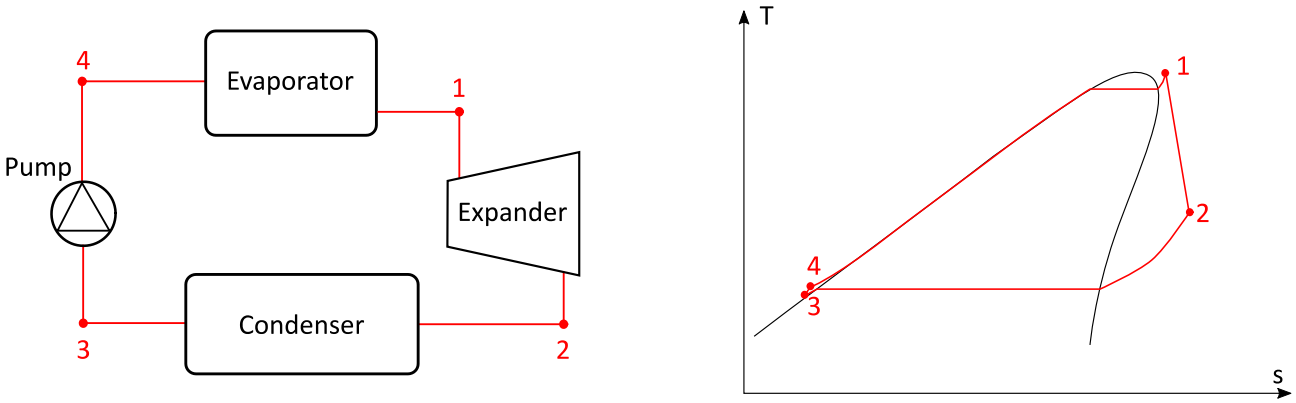

Figure A1 – Modelling of the Organic Rankine Cycle: outline schematic (left) and T-s diagram (right), showing the components and characteristic points of the cycle

The components and the main characteristic points of the ORC are presented in *Fig. A1*.

The low and high pressures of the ORC ($P_{low,ORC}$ and $P_{high,ORC}$) are calculated as the saturation pressures at the condensation temperature $T_{cond,ORC}$ and evaporation temperature $T_{evap,ORC}$, respectively:

$$P_{low,ORC} = P_{sat}\left(T_{cond,ORC}\right) \quad \text{(A.1)}$$

$$P_{high,ORC} = P_{sat}\left(T_{evap,ORC}\right) \quad \text{(A.2)}$$

, where the condensation temperature is determined according to the subcooling at the condenser outlet $\Delta T_{sub,ORC}$, the temperature pinch between the working fluid and the ambient sink at the condenser outlet $\Delta T_{HX,cond,ORC}$ and the ambient sink temperature T_{amb}:

$$T_{cond,ORC} = T_{amb} + \Delta T_{sub,ORC} + \Delta T_{HX,cond,ORC} \quad \text{(A.3)}$$

The evaporation temperature is determined according to the superheating at the evaporator outlet $\Delta T_{sup,ORC}$, the temperature pinch between the working fluid and the hot source at the evaporator outlet $\Delta T_{HX,evap,ORC}$ and the hot source temperature T_{hot}:

$$T_{evap,ORC} = T_{hot} - \Delta T_{sup,ORC} - \Delta T_{HX,evap,ORC} \quad \text{(A.4)}$$

The expansion of the working fluid in the expander and the pressurization of the working fluid in the pump are described by isentropic efficiencies $\eta_{is,e,ORC}$ and $\eta_{is,p,ORC}$.

The thermodynamic states of the characteristic points of the ORC are determined considering the equations listed in *Table A1*. Pressure drops are neglected.

	P	T	h
1ORC	$P_1 = P_{high,ORC}$	$T_1 = T_{hot} - \Delta T_{HX,evap,ORC}$	$h_1 = h(P_1, T_1)$
2ORC	$P_2 = P_{low,ORC}$	$T_2 = T(P_2, h_2)$	$h_2 = h_1 - \eta_{is,e,ORC}.\left(h_1 - h_{2,is}\right)$
3ORC	$P_3 = P_{low,ORC}$	$T_3 = T_{amb} + \Delta T_{HX,cond,ORC}$	$h_3 = h(P_3, T_3)$
4ORC	$P_4 = P_{high,ORC}$	$T_4 = T(P_4, h_4)$	$h_4 = h_3 + \frac{h_{4,is} - h_3}{\eta_{is,p,ORC}}$

Table A1 – Organic Rankine Cycle: model equations

The energy efficiency of the ORC, η_{ORC}, is calculated by:

$$\eta_{ORC} = \frac{|W_{ORC}|}{Q_{hot,ORC}} = \frac{(h_1 - h_2) - (h_4 - h_3)}{h_1 - h_4} \quad \text{(A.5)}$$

Electrochemical batteries

The energy efficiency of the electrochemical batteries η_{Bat} is defined by:

$$\eta_{Bat} = \frac{|W_D|}{W_C} \quad \text{(A.6)}$$

Regarding the depth of discharge of the batteries, Guena et al. [23] showed that it ranges between 0.5 and 0.8. Their results also suggest that cycling at reduced depth of discharge significantly improves the cycle life of the batteries: therefore, depth of discharge is a trade-off between the number of cycles and the storage density. Since thermochemical systems have a long lifetime, the depth of discharge of the batteries in the alternative system is set at 0.5, in order to maximize the number of cycles.

Refrigeration machine

The refrigeration machine (shown in *Fig. A2*) is a mechanically driven vapour compression chiller. In this cycle the vapour refrigerant is compressed from low pressure to high pressure, then it is

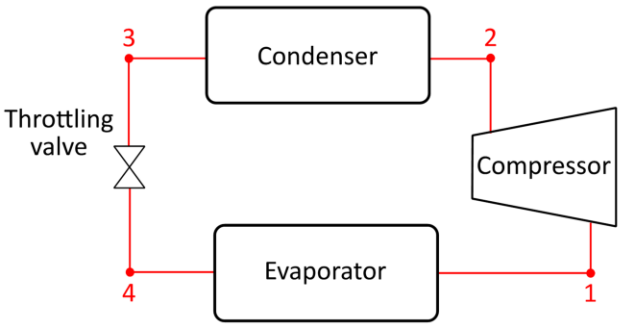

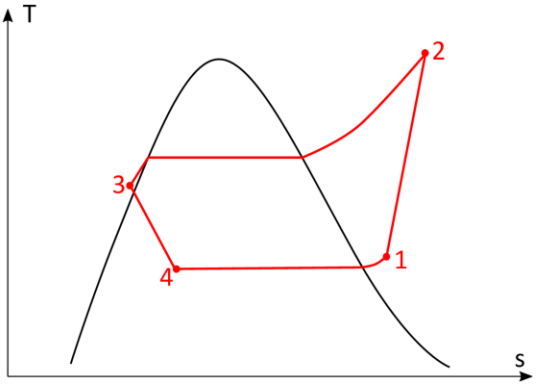

condensed and subcooled in the condenser. The liquid refrigerant is then throttled to the low pressure, and it is evaporated and superheated in the evaporator producing the refrigeration effect.

Figure A2 – Modelling of the vapour compression chiller: outline schematic (left) and T-s diagram (right), showing the components and characteristic points of the cycle

The low and high pressures of the refrigeration cycle ($P_{low,Ref}$, $P_{high,Ref}$) are calculated as the saturation pressures at the evaporation temperature $T_{evap,Ref}$ and the condensation temperature $T_{cond,Ref}$, respectively:

$$P_{low,Ref} = P_{sat}(T_{evap,Ref}) \quad (A.7)$$

$$P_{high,Ref} = P_{sat}(T_{cond,Ref}) \quad (A.8)$$

, where the evaporation temperature is determined according to the superheating at the evaporator outlet $\Delta T_{sup,Ref}$, the temperature pinch between the working fluid and the cold source at the evaporator outlet $\Delta T_{HX,evap,Ref}$ and the cold source temperature T_{cold}:

$$T_{evap,Ref} = T_{cold} - \Delta T_{sup,Ref} - \Delta T_{HX,evap,Ref} \quad (A.9)$$

The condensation temperature is determined according to the subcooling at the condenser outlet $\Delta T_{sub,Ref}$, the temperature pinch between the working fluid and the ambient sink at the condenser outlet $\Delta T_{HX,cond,Ref}$ and the ambient sink temperature T_{amb}:

$$T_{cond,Ref} = T_{amb} + \Delta T_{sub,Ref} + \Delta T_{HX,cond,Ref} \quad (A.10)$$

The compression of the working fluid in the compressor is described by an isentropic efficiency $\eta_{is,c,Ref}$.

The expansion of the working fluid in the throttling valve is isenthalpic.

The thermodynamic states of the characteristic points of the refrigeration cycle are determined considering the equations listed in *Table A2*.

	P	T	h
1_{Ref}	$P_1 = P_{low,Ref}$	$T_1 = T_{cold} - \Delta T_{HX,evap,Ref}$	$h_1 = h(P_1, T_1)$
2_{Ref}	$P_2 = P_{high,Ref}$	$T_2 = T(P_2, h_2)$	$h_2 = h_1 + \frac{h_{2,is} - h_1}{\eta_{is,c,Ref}}$
3_{Ref}	$P_3 = P_{high,Ref}$	$T_3 = T_{amb} + \Delta T_{HX,cond,Ref}$	$h_3 = h(P_3, T_3)$
4_{Ref}	$P_4 = P_{low,Ref}$	$T_4 = T(P_4, h_4)$	$h_4 = h_3$

Table A2 – Vapour compression chiller: model equations

The Coefficient of Performance of the refrigeration cycle COP_{Ref} is defined by:

$$COP_{Ref} = \frac{Q_{cold,Ref}}{W_{Ref}} = \frac{h_1 - h_4}{h_2 - h_1} \quad (A.11)$$